Dicle University Journal of Engineering

https://dergipark.org.tr/tr/pub/dumf
duje.dicle.edu.tr

Research Article

Thermal Performance Analysis of Photovoltaic Panels in Bitlis: Effect of Backsheet Material and Angled Fins

Yunus SAYAN[1*], Emin EL[2]

[1] Bitlis Eren University, Mechanical Engineering Department, ysayan@beu.edu.tr, Orcid No: 0000-0002-0871-6842
[2] Bitlis Eren University, Mechanical Engineering Department, eel@beu.edu.tr, Orcid No: 0000-0001-6596-9654

ARTICLE INFO

Article history:

Received 9 October 2025
Received in revised form 21 April 2026
Accepted 17 June 2026
Available online 10 July 2026

Keywords:

Photovoltaic panels, Thermal performance, Aluminum backsheet, Angled fins, Steady-state analysis

Doi: 10.24012/dumf.1800395

* Corresponding author

ABSTRACT

This study evaluates the thermal performance of five photovoltaic PV panels using steady-state thermal analysis in ANSYS. The panels include a standard PET backsheet panel, a PET + aluminum backsheet panel, a panel with only aluminum backsheet, and two finned configurations: one with PET + aluminum backsheet with angled fins, and another with only an aluminum backsheet with angled fins. Standard PET panels exhibited the highest PV cell temperatures (69.782 °C maximum, 60.746 °C minimum), while the PET + aluminum backsheet panel showed modest improvement (68.848 °C maximum, 62.93 °C minimum) due to enhanced lateral heat transfer. The panel with only aluminum backsheet displayed similar moderate reductions, confirming that PET alone has limited influence on thermal performance. The most significant temperature decreases and the most uniform thermal distribution were observed in the finned panels; the panel with only aluminum backsheet and angled fins reached PV cell temperatures of 58.503 °C maximum and 55.811 °C minimum. Thermal mitigation in the optimized finned design improved electrical efficiency from 17.94% to 18.78%, representing a 4.68% relative performance gain over the standard module under the specific environmental conditions of Bitlis. These results demonstrate that integrating angled fins with an aluminum backsheet effectively reduces localized heating, minimizes temperature gradients, and improves PV panel thermal reliability. However, these thermal improvements come at the cost of increased panel mass, rising from 26.54 kg in the standard PET panel to 39.797 kg in the finned aluminum design, highlighting the need to balance thermal benefits against structural and installation considerations.

Introduction

Energy is a fundamental element for the sustainability of human activities and has become an indispensable need for global economies [1]. Nations' level of development strongly correlates with their energy consumption levels [1], [2]. Rising population, higher living standards, growing industrialization, and rapid urbanization lead to significant growth in energy demand [3], [4].

Currently, about 75% of global energy demand is met by fossil fuels, causing major environmental challenges like greenhouse gas emissions and global warming. To address this, the world is undergoing a green transition, shifting from fossil-based systems to renewable resources with the goal of a fully sustainable energy future [1], [5]. Among renewable energy sources, solar energy stands out as one of the most widely used energy types thanks to its cleanliness, accessibility, sustainability, and unlimited potential [6], [7].

Solar energy can be used in a variety of applications, such as generating electricity through photovoltaic (PV) modules [8]–[10], providing hot air with solar air heaters [11], [12], drying vegetables and other agricultural products using solar air dryers [13], [14], providing drinking water with solar desalination units [15], [16] and cooking with solar cookers [17].

Solar photovoltaic cells have emerged as the primary technology for green electricity generation, providing significant flexibility in terms of installation with the capacity to generate energy using direct sunlight. However, efficiency losses caused by high cell temperatures limit the potential of PV cells [18]. Therefore, researchers have developed various techniques to improve the performance of photovoltaic cells and have extensively investigated possible solutions [19], [20].

Cooling systems are essential for enhancing the power output and efficiency of PV panels. These systems are classified as passive, active, or hybrid. Passive cooling relies on natural convection without extra energy use, offering simplicity and low cost. Active cooling uses forced convection and requires additional energy. Hybrid systems combine both natural and forced convection, also consuming energy for cooling [21]. Various techniques have been developed within these categories to enhance PV performance, including the use of phase change materials (PCM) [19], [20], thermoelectric coolers [22], thermoelectric generators [23] and nanofluids [24].

Some recent studies in this field include the work of H. Shawish et al., who studied two PCM-based passive cooling systems for PV panels, finding that the porous container reduced temperature by 3.40 °C and improved efficiency by

3.56% in winter, while the finned container reduced temperature by 3.42 °C and increased efficiency by 6.58% in summer [25]. A. Keçebaş et al. investigated ethanol-based PCM-integrated PV cooling systems and found that a 2 cm thick ethanol-filled absorber reduced front and back surface temperatures to 51 °C and 45 °C, increasing electrical and thermal efficiencies to 18% and 22%, respectively [26]. Hesham S. Abdelmohsen et al. compared two cooling techniques to improve PV performance. The first method used intermittent humidified air flowing from the bottom to the top of a 250 W panel to cool and clean the panel surface, reducing its temperature by 26 °C and increasing electrical output by 7.3%. The second method applied a water jacket with evaporative cooling to the back of a 50 W panel, lowering its temperature by 30 °C and boosting electrical output by 9.8% [27]. M. A. Bashir and H. M. Ali studied passive cooling systems with extended fin-based heat sinks for PV modules. Their numerical analysis showed that fin dimensions, number, spacing, and shape significantly affect heat dissipation. Rectangular pin fins achieved 33.77% and 41.4% higher heat dissipation than circular pin fins and long rectangular fins, respectively [28]. A. A. Hasan et al. conducted a CFD study on air-cooled heat sinks with different fin configurations to improve PV panel thermal performance. The study investigated the effects of fin number and spacing on airflow and heat dissipation, showing that increasing fin number enhances heat removal. The 11-fin design achieved the highest temperature drop (38.44 K), outperforming basic and intermediate designs, which were better than a finless model [29]. A. S. Soliman and P. Cheng studied PV cells integrated with PCM-filled finned heat sinks and compared them to conventional PCM enclosures. They found that the 6-fin design provided the most effective cooling, reducing PV cell temperatures by 27.9–31.11% and increasing electrical efficiency to 17.22–17.41%, outperforming standard PCM enclosures and demonstrating improved thermal and electrical performance [30]. A. Saxena et al. designed and tested an innovative heat sink for PV modules using water cooling, PCM-based cooling, or a combined approach. They found that the front-surface water-cooled system reduced surface temperature by 78.7% and increased efficiency by 22.8%, the rear-surface PCM system achieved a 25.7% temperature drop and 7.8% efficiency gain, and the combined system provided intermediate improvements of 36.8% and 10.3%, respectively [31]. I. Hossain et al. studied the impact of flat and wavy fin arrays on PV panel performance under both wind and still air conditions. They found that wavy fins, with a larger surface area, provided more effective cooling, 10 wavy fins reduced the panel temperature by 7 °C compared to 10 flat fins. Moreover, the 20-wavy-fin configuration improved electrical efficiency by 2% over the baseline, demonstrating the superior thermal and electrical performance of wavy fins [32].

In this study, the thermal performance of PV panels with different backsheet configurations was investigated to identify effective strategies for reducing PV cell temperatures and achieving uniform thermal distribution. Steady-state thermal analysis in ANSYS was conducted to compare a conventional PET-backed panel, an aluminum-backed panel, a PET + aluminum-backed panel, a panel with a PET + aluminum backsheet combined with angled fins, and a panel with an aluminum backsheet combined with angled fins. The novelty of this work lies in the combined evaluation of backsheet materials and angled fin configurations to optimize thermal management in PV panels, providing a practical guideline for passive cooling design.

Modeling

Geometrical Modeling and Material Properties

This study employed the TommaTech 550 Wp M10 144PM HC-MB solar panel (see Fig. 1A). In the analysis, the effects of cell fingers and busbars were neglected. Further technical specifications are available in the datasheet [33].

Fig. 1 illustrates five different photovoltaic panel configurations developed for this study. The first design (PV Panel 1) represents the standard module structure, consisting of tempered glass, ethylene vinyl acetate (EVA) encapsulant layers above and below the monocrystalline half-cut M10 silicon cells, a polyethylene terephthalate (PET) backsheet, and an anodized aluminum frame. The second design (PV Panel 2) contains the same layers as PV Panel 1, with the addition of an anodized aluminum sheet placed beneath the PET backsheet. The third configuration (PV Panel 3) replaces the PET layer entirely with an anodized aluminum backsheet. The fourth design (PV Panel 4) incorporates PET + an anodized aluminum backsheet combined with angled aluminum fins to enhance heat dissipation. Finally, the fifth configuration (PV Panel 5) is similar to PV Panel 4 but excludes the PET layer, leaving only the anodized aluminum backsheet with fins. These alternative configurations aim to investigate the influence of aluminum backsheet integration and fin-assisted cooling on reducing PV module temperature under the hottest critical day condition between 2011 and 2024 in Bitlis.

The PV panel with aluminum frame has a width of 1136 mm and a height of 2280 mm. The layer thicknesses are as follows: tempered glass, 3.2 mm; EVA, 0.4 mm; silicon cells, 0.18 mm; PET, 0.3 mm; and anodized aluminum backsheet, 1 mm. Additional geometric details are provided in Fig. 1.

Table 1 presents the material properties used in the modeled PV panels. In the simulations, the EVA layer was simplified as a fully transparent medium. In addition, ground effects were incorporated into the analysis by assuming the ground surface to represent an uncultivated field.

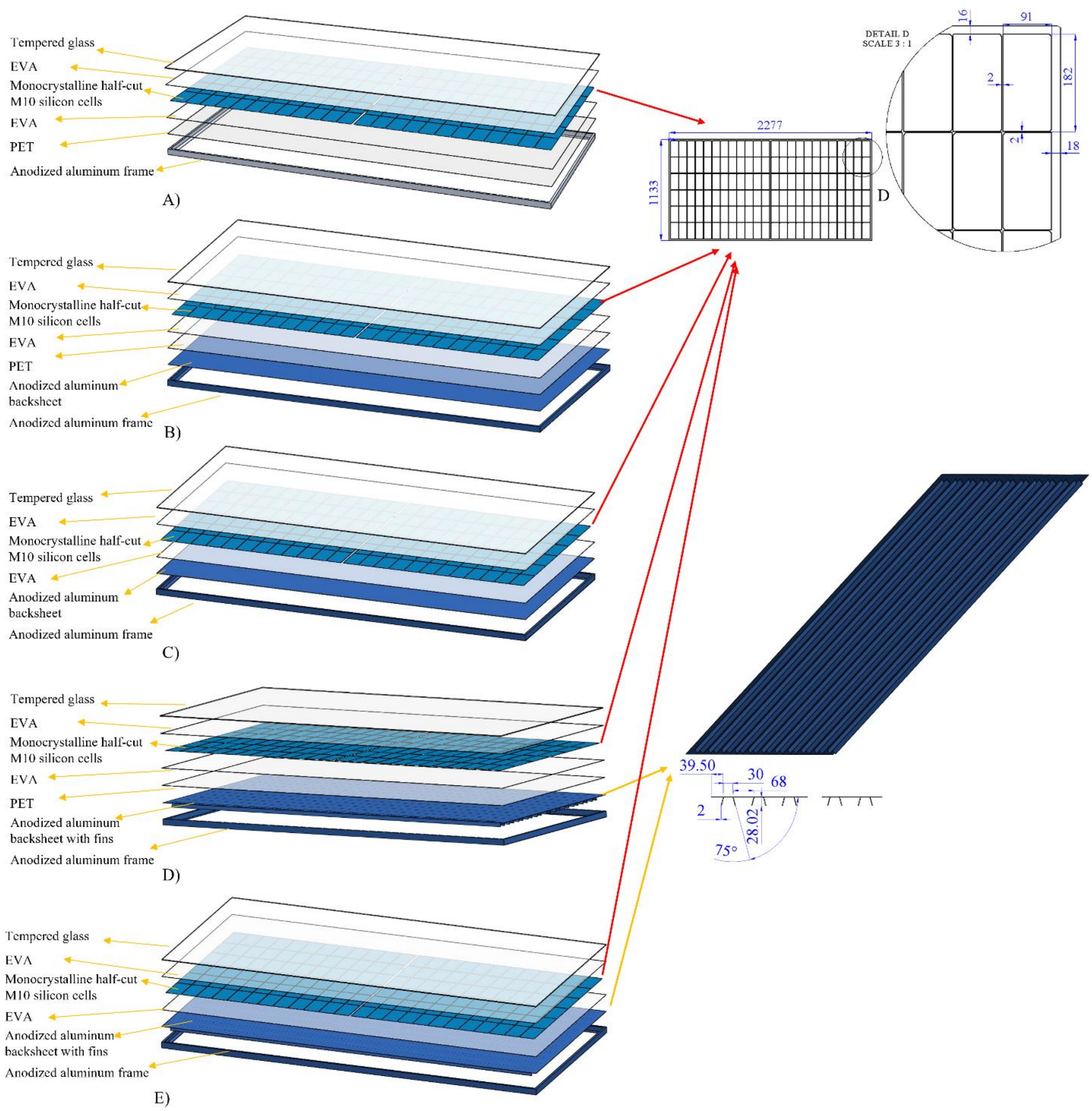

Figure 1. Schematic representation of the TommaTech 550 Wp M10 144PM HC-MB photovoltaic panel with five design configurations: (A) PV Panel 1 – standard panel with PET backsheet; (B) PV Panel 2 – panel with PET backsheet and additional anodized aluminum sheet; (C) PV Panel 3 – panel with anodized aluminum backsheet only (PET removed); (D) PV Panel 4 – panel with PET+ anodized aluminum backsheet with angled fins; (E) PV Panel 5 – panel with anodized aluminum backsheet with angled fins, without PET (model geometries generated in SolidWorks).

Table 1. Material properties of the layers used in the photovoltaic panel simulations.

	Thermal conductivity (k), (W/m C°)	Specific heat capacity (c_p), (J/ kg C°)	Density (ρ), (kg /m^3)	Emissivity (ε)	Absorptivity (α)	Reflectivity (ρ)	Transmittivity (τ)
Tempered glass	1 [34]	720 [34]	2500 [34]	0.84 [34]	0.04 (Calculated)	0.04 [35]	0.92 [34], [36]
Ethylene vinyl acetate (EVA) encapsulant top and bottom	0.35 [37]	2090 [37]	945 [37]	-	0	0	1 [37]
Monocrystalline half-cut M10 silicon cell	148 [37]	700 [37]	2330 [37]	-	0.97 [37]	0.03 [37]	0 (Calculated)
Polyethylene Terephthalte film (PET) backsheet	0.31 [38]	1200 [38]	1360 [38]	0.82 [39]	0.13 (Calculated)	0.83 [40]	0.04 (for 0.3 mm thickness) [41]
Anodized aluminum (for support and backsheet)	227 [42]	900 [42]	2705 [42]	0.84 [43]	0.14 [43]	0.86 [44]	0 (Calculated)
Ground reflection (Uncultivated fields)	-	-	-	-	-	0.26 [45]	-

Numerical Modeling

According to PV Education, for a fixed tilt angle, the highest annual power output is obtained when the tilt angle is set equal to the latitude of the location [46]. Bitlis is located at a latitude of 38.4° N and a longitude of 42.1° E [47]. Therefore, the tilt angle of the photovoltaic panels was chosen as 38.4° (see Fig. 2), corresponding to the latitude of the site.

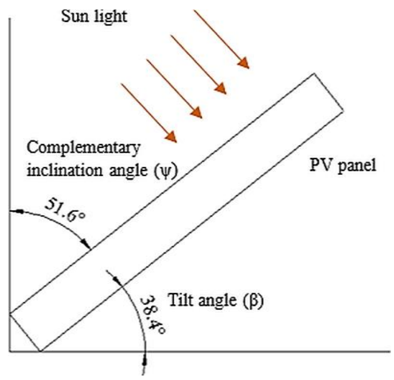

Figure 2. Tilt angle of the photovoltaic panels set equal to the latitude of Bitlis (38.4° N).

A solar panel, when exposed to sunlight, attains a temperature higher than the surrounding environment due to the absorbed solar radiation. Its thermal equilibrium is determined by the ambient temperature (T_E, *°C or K*), the incident solar heat flux (Q_{Source}, *W*), and the absorption coefficient of materials (α, dimensionless). This balance is maintained through the combined effects of radiation, convection, and layer-to-layer conduction, each of which depends on both the panel surface temperature (T_P, *°C or K*) and the environmental temperature.

At thermal equilibrium, the energy absorbed from the source (Q_{Source}) is equal to the energy released by the panel through radiation ($Q_{Radiation}$, *W*) and convection ($Q_{Convection}$, *W*) [37]:

$$Q_{Source} = Q_{Convection} + Q_{Radiation} \tag{1}$$

Convective heat transfer from the panel surface to the surrounding air can be estimated using Newton's law of cooling [43]:

$$Q_{Convection} = hA(T_P - T_E) \tag{2}$$

where h is the convective heat transfer coefficient ($W/m^2{\cdot}K$) and A is surface area exposed to the fluid (m^2).

Radiative heat exchange is defined by the Stefan–Boltzmann law:

$$Q_{Radiation} = \varepsilon\sigma A(T_P^4 - T_E^4) \tag{3}$$

where ε is the emissivity of the surface (dimensionless, 0–1), A is the radiation emitted or absorbed surface area (m^2) and σ is the Stefan–Boltzmann constant (W/m^2K^4).

In addition to these external exchanges, internal heat conduction through the PV layers (glass, encapsulant, solar cells, backsheet) determines the temperature distribution within the module. This conduction can be expressed by Fourier's law:

$$Q_{conduction} = -kA\frac{dT}{dx} \tag{4}$$

where k denotes the thermal conductivity of the layer material (*W/mK*), A is the cross-sectional area (perpendicular to the direction of heat transfer, m^2), and dT/dx represents the temperature gradient across the layers (*K/m*). Conduction is used to calculate the temperature profile across the panel layers, while the global energy balance considers only radiation and convection at the surfaces.

As mentioned above, the maximum annual power generation is achieved when the panel tilt angle is aligned with the latitude of the location; therefore, PV panels are inclined in this manner to optimize energy output. Thus, in order to accurately calculate the heat transfer from both the top and bottom surfaces of the PV panel, it is necessary to determine the heat transfer coefficient for inclined surfaces. In this process, both natural and forced convection mechanisms are taken into account to ensure a more comprehensive and precise evaluation.

For natural convection, the Nusselt number can be estimated using simple empirical correlations [43]:

$$Nu = \frac{hL_c}{k} = CRa_L^n \quad (5)$$

where:

- Nu = Nusselt number (dimensionless)
- L_c= characteristic length of the surface (m)
- k = thermal conductivity of the fluid ($W/m \cdot K$)
- C,n = empirical constants depending on surface geometry and flow regime
- Ra_L = Rayleigh number (dimensionless)

where Ra_L is the Rayleigh number, defined as the product of the Grashof (Gr_L, dimensionless) and Prandtl (Pr, dimensionless) numbers:

$$Gr_L = \frac{g\beta(T_P - T_E)L_c^3}{v^2} \quad (6)$$

$$Ra_L = Gr_L Pr = \frac{g\beta(T_P - T_E)L_c^3}{v^2} Pr \quad (7)$$

where:

- g = gravitational acceleration (m/s^2)
- β = thermal expansion coefficient of the fluid ($1/T_f$, $1/K$)
- v = kinematic viscosity of the fluid (m^2/s)

The values of the constants C and n depend on the surface geometry and the flow regime, which is determined by the range of the Rayleigh number. In general, n takes the value of 1/4 laminar flow and 1/3 for turbulent flow, while the constant C is usually less than 1.

The film temperature is defined as $T_f=1/2(T_P + T_E)$ and all fluid properties are evaluated at this temperature.

Nusselt Number for Natural Convection on Inclined PV Panel Surfaces

Natural convection heat transfer from isothermal flat surfaces, such as PV panel surfaces, depends on their orientation relative to the surrounding fluid. To evaluate natural convection heat transfer from isothermal flat plates at an inclination, correlations of the following form are used [48]:

$$Nu_{(\psi)} = C_{(\psi)}(\Pi_N)^n \quad (8)$$

$$\Pi_N = Ra/(1 + 0.492/Pr) \quad (9)$$

In these expressions:

- $Nu_{(\psi)}$ is the Nusselt number as a function of the Complementary inclination angle ψ,
- $C_{(\psi)}$ and n are empirical constants dependent on surface geometry and flow regime.

These correlations are applicable for any characteristic length, for inclination angles between 0° (vertical) and 90° (horizontal), and for Prandtl numbers ranging from 0.001 to very large values, providing a general method for estimating natural convection heat transfer from flat surfaces.

For the upper surface, the critical Grashof number is [48]:

$$Gr_{cr1} = \frac{1}{Pr} 10^{(5\cos\psi + 4.9)} \quad 0° < \psi \le 90° \quad (10)$$

$$C_{(\psi)} = 0.057 + 0.098(\sin\psi)^{1/3} \quad (11)$$

$$0° < \psi \le 90° \quad Gr > Gr_{cr1} \; for \; \psi \ge 21.42°$$

For the bottom surface, the critical Grashof numbers are:

$$Gr_{cr2} = \frac{1.7\ 10^{11}}{Pr} e^{(\psi \ln 2)/90} \quad 0° \le \psi \le 90° \quad (12)$$

$$Gr_{(cr3)} = \frac{10^{9.9}}{Pr} e^{(\psi \ln 2)/90} \quad 0° \le \psi \le 90° \quad (13)$$

$$Gr_{cr2} > Gr > Gr_{cr3}$$

$$C_{(\psi)} = 0.046 + 0.011(\cos\psi)^{1/3} \quad (14)$$

Nusselt Number for Forced Convection from Inclined PV Panel Surfaces

For forced convection from the upper and bottom surfaces of the PV panel and any direction of the wind, the following correlations can be used [48]:

$$Nu = 0.664Re^{1/2}Pr^{1/3} \quad for = Re \le 5.10^5 \quad (15)$$

$$Nu = \left(0.037R^{4/5} - 871\right)Pr^{1/3} for \; Re > 5.10^5 \quad (16)$$

where Nu is the corresponding Nusselt number, Re is the Reynolds number, V_w is the wind velocity and v is the kinematic viscosity of the air.

For forced convection, the Reynolds number is given as

$$Re = \frac{V\,L_c}{v} \quad (17)$$

Once the average Nusselt number—and consequently the corresponding average convective heat transfer coefficient—has been determined, the convective heat transfer rate from a solid surface at uniform temperature T_P to the surrounding fluid, accounting for both natural and forced convection, can be expressed using Newton's law of cooling (Equation 2).

The relative importance of natural convection in a PV panel can be assessed using the ratio Gr/Re^2. If Gr/Re^2>>1, natural convection predominates, whereas if Gr/Re^2<<1, forced convection dominates. When Gr/Re^2≈1, both natural and forced convection contribute significantly to the overall heat transfer [43], [49]. In this study, the calculated value is

0.1878, indicating that both natural and forced convection should be considered for the upper and bottom surfaces of the panel when estimating the convective heat transfer coefficient.

In this study, the convective heat transfer coefficient for the inclined PV panel surfaces was calculated using the mixed convection approach, where the Nusselt number is determined by combining forced and natural convection contributions as [43]

$$Nu_{Mixed} = \left(Nu_{forced}^3 + Nu_{natural}^3\right)^{1/3} \quad (18)$$

allowing both mechanisms to be accounted for simultaneously in the heat transfer analysis.

Thermal Effect on Electrical Performance

To quantify the practical benefits of the temperature reductions achieved through the proposed designs, the electrical efficiency (η) of the PV modules was estimated. Although the primary focus of this study is thermal management, calculating the projected efficiency recovery is essential to demonstrate the direct impact on power output. The temperature-dependent electrical efficiency was calculated using the widely accepted linear model proposed by Evans [50] and further reviewed by Skoplaki and Palyvos [51]:

$$\eta = \eta_{STC}[1 - \beta(T_c - T_{STC})] \quad (19)$$

Where: η_{STC} is the reference efficiency under Standard Test Conditions (STC:1000 W/m^2, 25°*C*), which is 21.28% for the TommaTech 550 Wp M10 module used in this study. β is the temperature coefficient of power, taken as 0.350%/°*C*) from the manufacturer's datasheet. Tc is the cell temperature obtained from the numerical simulations. T_{STC} is the reference temperature (25°*C*).

Operating and Input Parameters

In this study, Bitlis, Turkey, was selected as the research area. For the PV analysis, the maximum temperature measured between 2011 and 2024 was considered. This value, 34.6 °C, was recorded on July 20, 2021 (see Turkish State Meteorological Service [52], see Table 2) and was taken as the critical ambient temperature. Furthermore, based on Oral [53], the average wind speed in Bitlis during July is 3.6 m/s, and this value was adopted for the analysis. The solar radiation was assumed to be the standard 1000 W/m². In addition, the selected TommaTech 550 Wp M10 144PM HC-MB solar panel was assumed to generate 550 W of power. The absorptivity, emissivity, reflectivity, and transmissivity of each material, as listed in Table 1, were determined and incorporated into the ANSYS steady-state thermal analysis to accurately model the thermal behavior of the panel.

The convective heat transfer coefficients for the PV panel surfaces were calculated using mixed convection correlations, considering both top and bottom surfaces to account for natural and forced convection effects. In the analysis, a steady-state process without internal heat generation was assumed, and the thermal conductivity of the material was considered constant. To simplify the computational model for the finned backsheet, the convective heat transfer coefficient was determined based on flat-surface correlations and was assumed uniform over the entire surface of the fins. The detailed equations and intermediate steps used to compute these coefficients are summarized in Table 3, along with the resulting values of *h* for each surface. These coefficients were subsequently employed in the thermal analysis to estimate heat dissipation and temperature distribution across the panel, providing a more accurate representation of its thermal behavior under operational conditions.

Table 2. Maximum and minimum ambient temperatures in Bitlis (2011–2024) in °C used for PV analysis [52].

BITLIS	January	February	March	April	May	June	July	August	September	October	November	December
Maximum Temp.	10,1	21,9	16,7	22,3	27,4	31,5	34,6	33,3	34,0	26,4	21,7	13,3
Minimum Temp.	-24.1	-20.0	-20.3	-10.0	0.1	5.2	8.1	20.07.2021	0.0	-0.6	-10.0	-20.8

Table 3. Equations and computed values used to determine mixed convection heat transfer coefficients (h) for the top and bottom surfaces of the PV panel.

T_P (°C)	T_E (°C)	T_f (°C)	k_{air} (W/m °C)	ν_{air} (m²/s)	Pr_{air}	V_{air} (m/s)
≈70 (Calculated after several iteration)	34.6	52.3	0.0275179	1.8205e-5	0.722202	3.6 [53]
Lc (m)	**β (1/K)**	**Re**	**Gr_{L_c}**	**Ra_{L_c}**	**Gr_{L_c} Re^{-2}**	
2.28	0.003074	450855.241	38176164747.4	27570902533	0.1878097	
Critical Grashof number			**Natural convection for upper surface**		**Natural convection for bottom surface**	
Gr_{cr1}	**Gr_{cr2}**	**Gr_{cr3}**	**Nu**	**h W/m °C**	**Nu**	**h W/m °C**
140307283	350252114178.71	16365596680	374.367282	4.518333961	140.7134783	1.69830677

Forced convection for upper and bottom surfaces		Mixed Nu for upper surface	Mixed h for upper surface (W/m °C)	Mixed Nu for bottom surface	Mixed h for bottom surface (W/m °C)
Nu	h (W/m °C)				
400.011861	4.82784491	488.362702	5.894173688	405.733792	4.89690435

Validation (mesh)

As presented in Table 4, the mesh validation study confirmed that the maximum temperature of the solar cells remains almost unchanged as the mesh is refined from 613002 elements (Order 1) to 902690 elements (Order 5), based on the results obtained for PV panel 1. The maximum variation observed across all mesh levels was only ±0.03%, indicating that the results are essentially mesh-independent. Since further refinement does not yield significant improvements in accuracy but increases computational demand, the first-order mesh with 613002 elements was selected for the subsequent analyses to achieve an optimal balance between accuracy and efficiency.

Table 4. Mesh independence analysis (Variations in maximum temperature of solar cells).

Order	Number of elements	Simulation maximum temperature from solar cells °C	Temperature changes from initial simulation value (Order 1) %
1	613002	69.764	
2	697242	69.701	-0.09
3	764306	69.774	0.014
4	844693	69.782	0.026
5	902690	69.785	0.03

Results and Discussion

Fig. 3 presents the steady-state glass surface temperature distributions of the five PV panels. For PV Panel 1, which employs only a PET backsheet, the maximum and minimum glass temperatures are 69.38 °C and 59.54 °C, respectively. Cooler regions occur along the glass areas in contact with the aluminum frame, while the highest values appear at the centers of the two cell sections; although the glass is continuous, the configuration of 144 cells arranged in two groups of 72 separated by an intercell gap results in two distinct hot regions.

In PV Panel 2, an aluminum sheet is added on top of the PET backsheet to enhance heat dissipation. Although aluminum has a much higher thermal conductivity (227 W/m°C) than PET (0.31 W/m°C), adding it as an extra layer slightly increases the total series thermal resistance, as the thin sheet still introduces a finite resistance. Its primary effect is to improve lateral heat spreading, which reduces local hot spots but warms cooler areas, thereby increasing the minimum temperature compared to Panel 1. The slightly higher emissivity of aluminum (0.84 vs. 0.82 for PET) also contributes modestly to additional radiative cooling. Consequently, the glass surface temperatures range from 61.61 °C (minimum) to 68.46 °C (maximum), compared to 59.54 °C and 69.38 °C for PV Panel 1.

In PV Panel 3, the PET backsheet is completely removed, leaving only the aluminum layer as the backsheet. The maximum and minimum glass surface temperatures are 68.30 °C and 61.57 °C, respectively, showing a range very similar to PV Panel 2. This indicates that removing the PET layer has almost no effect on the temperature distribution, as its thermal resistance is minor relative to the overall module.

In PV Panel 4, angled aluminum fins are added to the aluminum backsheet to enhance convective cooling. This results in a further reduction of glass surface temperatures, with a maximum of 58.53 °C and a minimum of 54.66 °C. PV Panel 5 is similar to PV Panel 4 but has the PET layer removed, leaving only the aluminum backsheet with fins. The maximum and minimum glass temperatures for PV Panel 5 are 58.24 °C and 54.65 °C, respectively, showing that removing the PET layer has almost no effect on the temperature distribution. The temperature difference between the maximum and minimum for PV Panels 4 and 5 is smaller than that of the previous panels, indicating that the addition of fins not only lowers temperatures but also narrows the temperature distribution. Unlike the marginal changes observed in Panel 2 and 3, the addition of fins significantly improves thermal uniformity and demonstrates the effectiveness of enhanced backsheet cooling.

Fig. 4 shows the steady-state EVA 1 temperature distributions of the five PV panels, which closely follow the glass temperature patterns shown in Fig. 3. The EVA 1 maximum and minimum temperatures for PV Panels 1–5 is 69.78–59.39 °C, 68.85–62.50 °C, 68.68–62.58 °C, 58.80–55.31 °C, and 58.50–55.32 °C, respectively. The addition of aluminum backsheets and angled fins progressively lowers the EVA 1 temperatures and narrows the temperature range, indicating improved thermal uniformity across the EVA 1 layer.

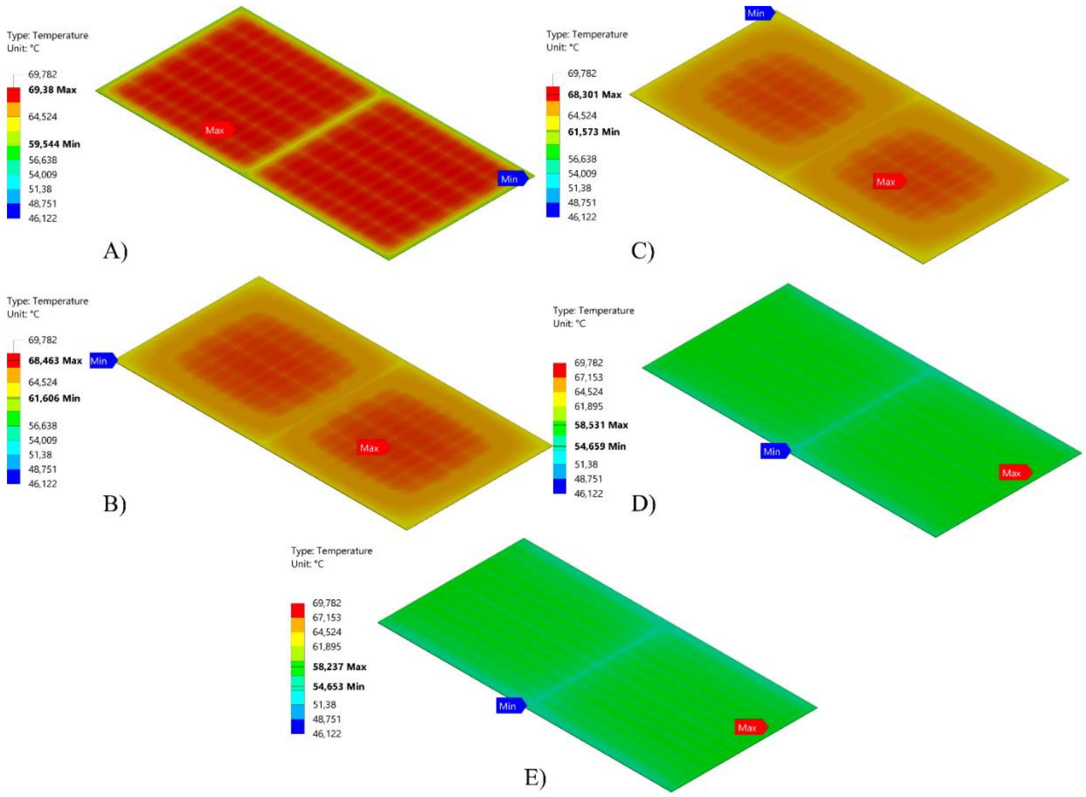

Figure 3. Smooth contour plots of glass surface temperature at steady state for (a) PV Panel 1, (b) PV Panel 2, (c) PV Panel 3, (d) PV Panel 4, and (e) PV Panel 5. A uniform color scale (min–max shown on the colorbar) was applied across all panels to allow direct comparison.

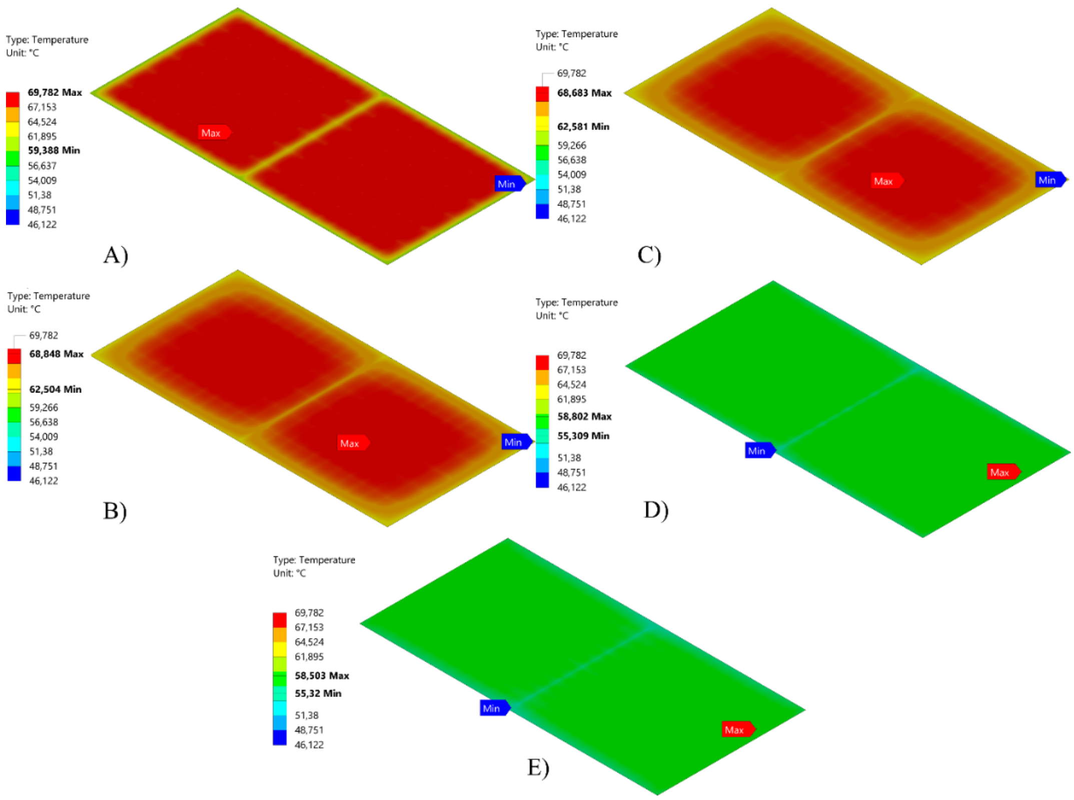

Figure 4. Contour representations of steady-state temperature over the EVA 1 layer for (a) PV Panel 1, (b) PV Panel 2, and (c) PV Panel 3, (d) PV Panel 4, and (e) PV Panel 5. A common temperature scale is applied to each map to ensure comparability.

Fig. 5 presents the steady-state temperature distribution contours on the solar cell layer for PV Panels 1–5. The cell-level temperature distributions of PV Panel 1 and PV Panel 5 is also shown in Fig. 6 in order to compare the differences in thermal behavior between the two configurations more clearly. In Fig. 5, the use of a common color scale made it difficult to clearly visualize PV Panel 5, as it exhibits both lower maximum and minimum temperatures and a smaller temperature gradient compared to PV Panel 1. The maximum and minimum temperatures on the solar cell layer are as follows: PV Panel 1 — 69.782 °C and 60.746 °C; PV Panel 2 — 68.848 °C and 62.93 °C; PV Panel 3 — 68.683 °C and 62.939 °C; PV Panel 4 — 58.802 °C and 55.822 °C; PV Panel 5 — 58.503 °C and 55.811 °C. In all panels, the minimum temperatures are observed near the aluminum frame, while the highest temperatures occur at the centers of the two cell sections, each consisting of 72 cells (144 cells in total). As explained for the glass temperature distribution in Fig. 3, a similar pattern is observed here. The temperature difference between PV Panels 2 and 3 is minimal, indicating that the effect of PET on cell temperature reduction can be considered negligible. PV Panels 4 and 5 exhibit significantly lower operating temperatures due to the presence of fins on the aluminum backsheet, which enhance heat dissipation. The nearly identical temperature distributions of Panels 4 and 5 further suggest that PET has little impact in these finned configurations also.

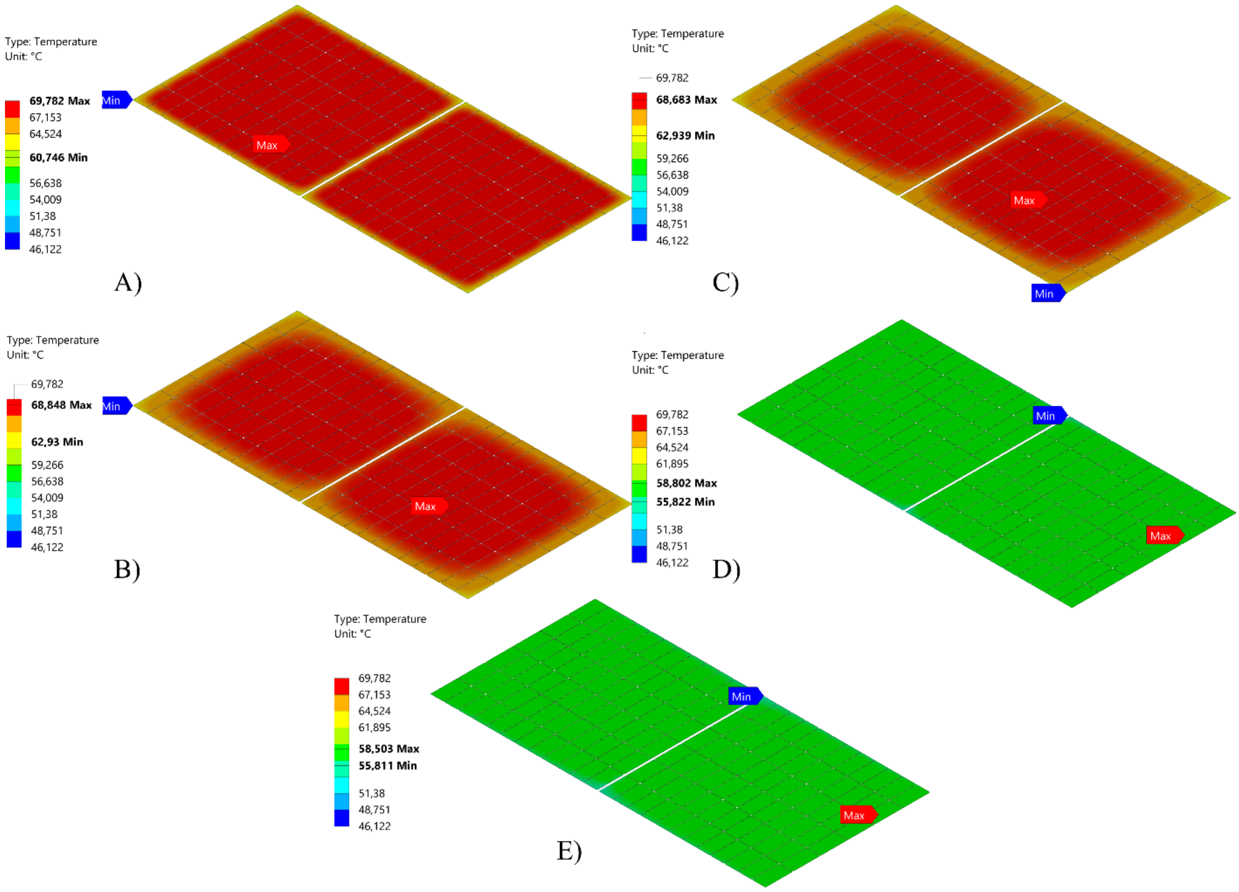

Figure 5. Temperature distribution contours on the solar cell layer at steady state for (a) PV Panel 1, (b) PV Panel 2, and (c) PV Panel 3, (d) PV Panel 4, and (e) PV Panel 5. A common color scale is used to emphasize differences between panels.

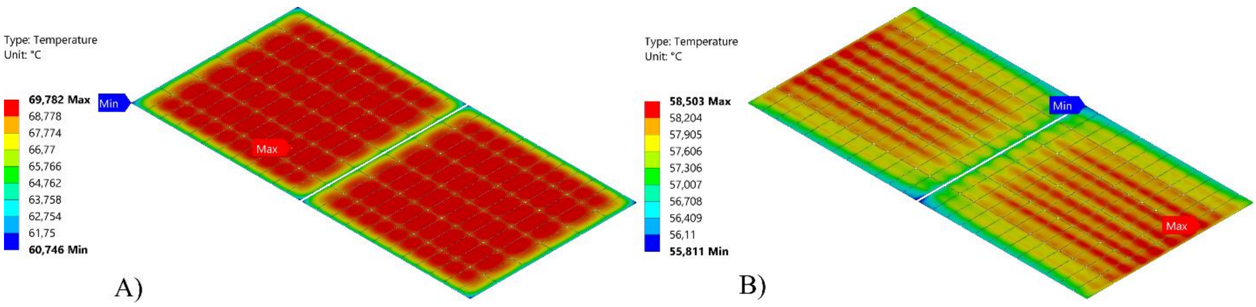

Figure 6. Direct comparison of cell-level temperature distributions: (A) PV Panel 1 and (B) PV Panel 5. The side-by-side representation clearly illustrates the temperature gradient in each panel and allows evaluation of the impact of aluminum backsheet and fin integration on thermal behavior.

For PV Panel 1, the EVA-2 layer reaches a maximum of 69.781 °C and a minimum of 46.122 °C, while the PET layer shows a maximum of 69.412 °C and a minimum of 46.224 °C (see Fig. 7 and Fig.8). By contrast, in PV Panel 2 the EVA-2-layer records 68.847 °C (maximum) and 62.625 °C (minimum), and the PET layer 68.462 °C (maximum) and 62.658 °C (minimum). These results indicate that PV Panel 1 experiences a much larger temperature gradient across the layers, whereas PV Panel 2 maintains a narrower range. The higher minimum temperature observed in PV Panel 2 can be explained by the presence of the aluminum backsheet, which enhances lateral heat conduction as we mentioned in previous paragraphs. This not only lowers the peak temperature but also prevents excessive cooling near the panel edges, thereby promoting a more uniform temperature distribution and reducing localized thermal stresses (see Fig. 7 and 8).

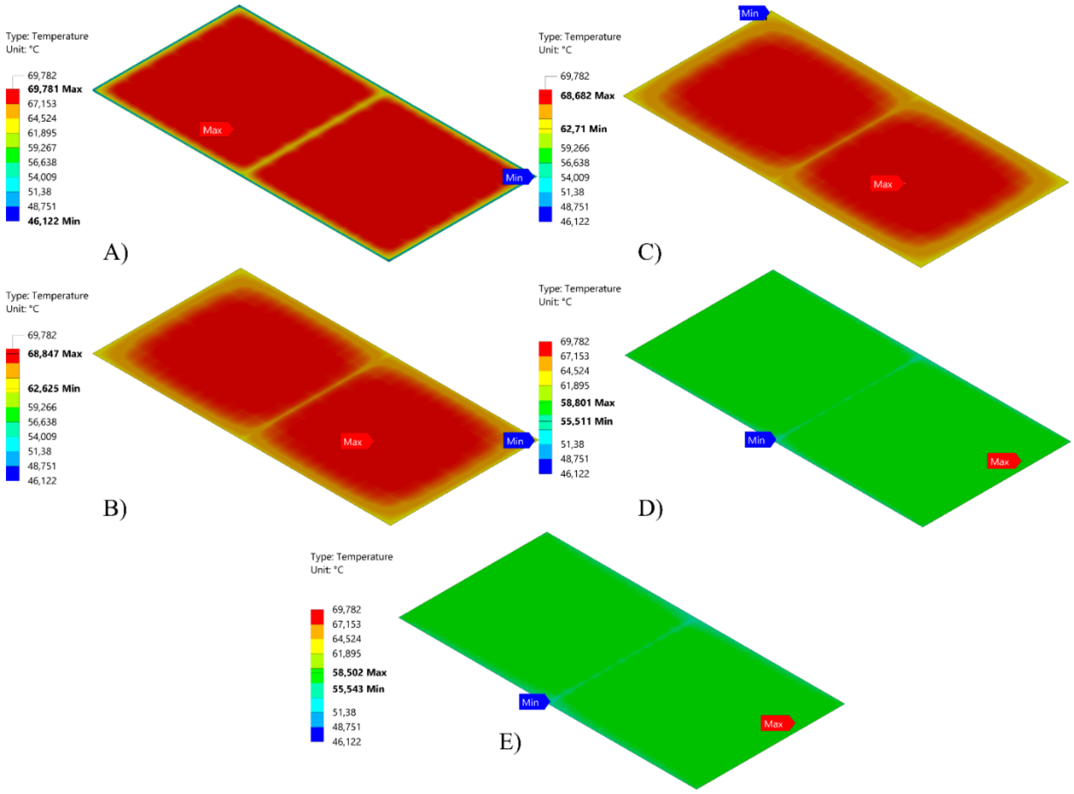

Figure 7. Contour plots showing steady-state temperature on the EVA 2 layer for (a) PV Panel 1, (b) PV Panel 2, and (c) PV Panel 3, (d) PV Panel 4, and (e) PV Panel 5. The same color scale is applied across all panels to facilitate direct comparison.

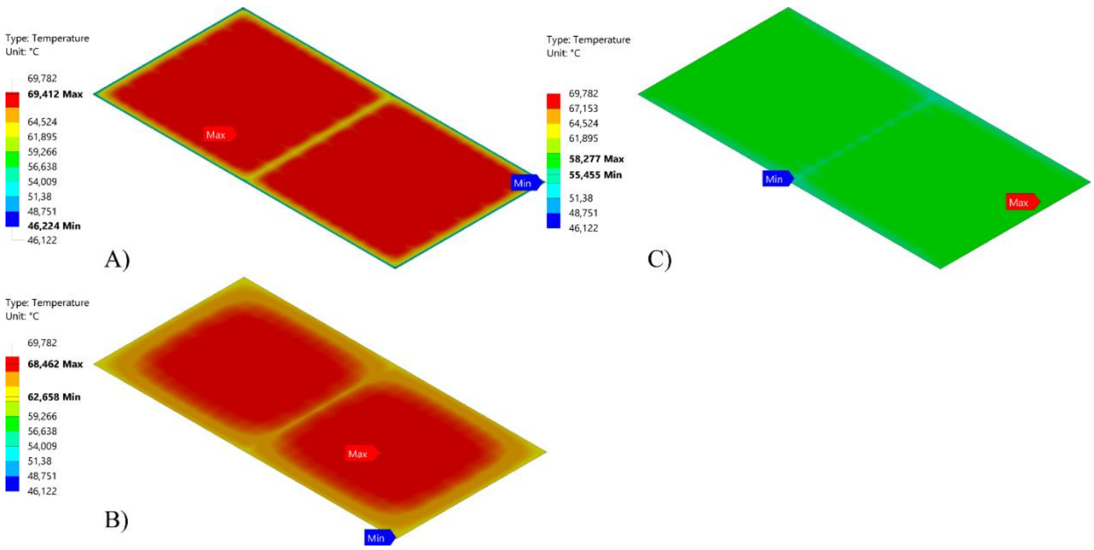

Figure 8. Steady-state temperature contour maps of the PET layer for (a) PV Panel 1, (b) PV Panel 2, and (c) PV Panel 4. A uniform color scale is used across all panels to enable direct comparison.

Fig. 9 presents the temperature distribution of the aluminum frame for PV Panels 1–5. For PV Panel 1, the maximum and minimum frame temperatures are 60.583 °C and 59.688 °C, respectively. PV Panel 2 records 64.267 °C (maximum) and 62.594 °C (minimum), while PV Panel 3 shows similar values of 64.367 °C and 62.67 °C. In contrast, PV Panels 4 and 5 exhibit noticeably lower frame temperatures, with PV Panel 4 ranging between 57.483 °C and 55.665 °C, and PV Panel 5 between 57.562 °C and 55.73 °C. These results indicate that Panels 2 and 3 operate with slightly higher aluminum frame temperatures due to reduced thermal gradients associated with the aluminum backsheet, while the incorporation of fins in Panels 4 and 5 enhances cooling efficiency, leading to the lowest frame temperatures among all configurations.

Fig. 10 illustrates the temperature distribution of the aluminum backsheet (with or without fins) for PV Panels 2–5. PV Panels 2 and 3 exhibit the highest temperatures, with maximum and minimum values of 68.136 °C and 62.671 °C, and 68.293 °C and 62.746 °C, respectively, showing a moderate temperature gradient across the sheet. In contrast, Panels 4 and 5 display lower temperatures, ranging from 57.878 °C to 55.184 °C for Panel 4 and 58.003 °C to 55.297 °C for Panel 5, with a smaller temperature gradient due to the fins enhancing lateral heat transfer. The comparison indicates that the fins in Panels 4 and 5 effectively reduce both the maximum temperature and the temperature gradient, improving thermal uniformity, whereas Panels 2 and 3 maintain higher temperatures and a more pronounced gradient in the aluminum backsheet.

For PV Panels 4 and 5, the maximum temperatures across the layers—from glass to EVA to cells and backsheet—are relatively close to each other. Similarly, the minimum temperatures also exhibit comparable values throughout the layers. This behavior is due to the efficient thermal contact between the layers and their material properties. Each layer is in direct contact with adjacent layers, which promotes effective heat transfer. Furthermore, the thinness of the layers limits significant vertical temperature gradients, and under steady-state conditions, the heat absorbed by the solar cells is efficiently conducted to and dissipated through the surrounding layers of the panels. The presence of fins on the aluminum backsheet in these panels further enhances heat dissipation, helping to maintain a uniform temperature distribution across all layers.

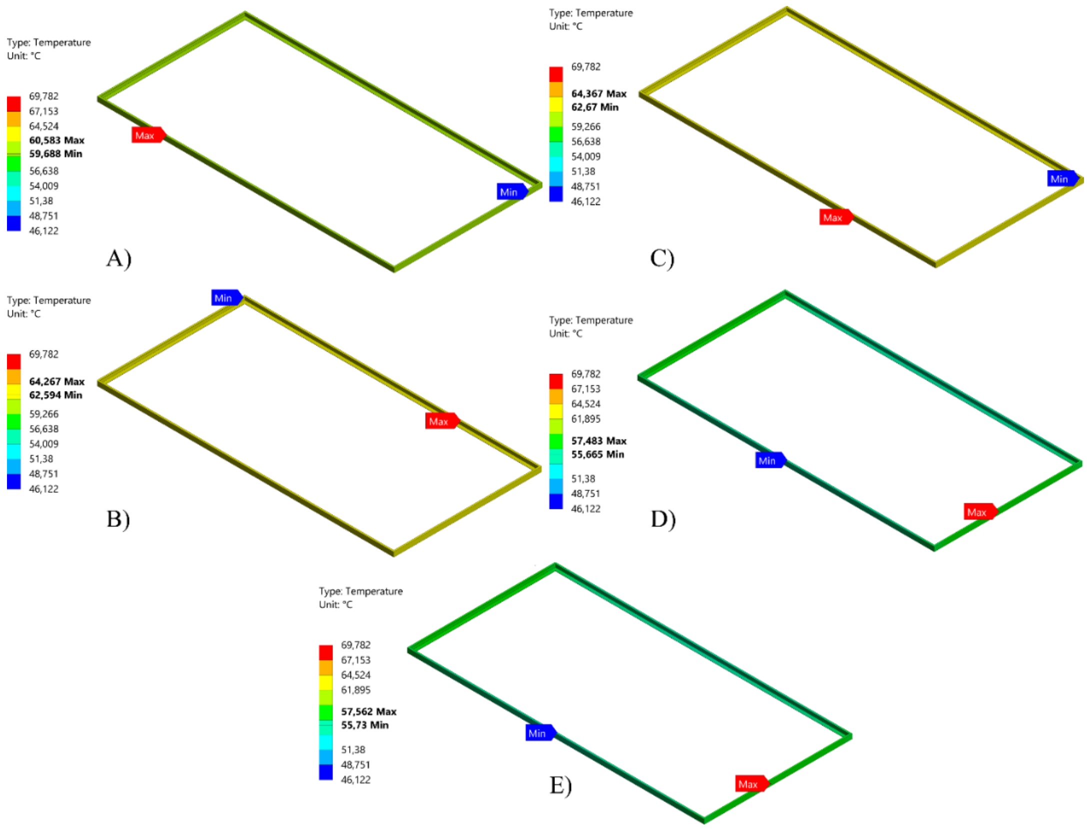

Figure 9**.** Steady-state temperature distribution on the aluminum frame for (a) PV Panel 1, (b) PV Panel 2, and (c) PV Panel 3, (d) PV Panel 4, and (e) PV Panel 5. The same color scale is applied across all panels to allow direct comparison of surface temperatures.

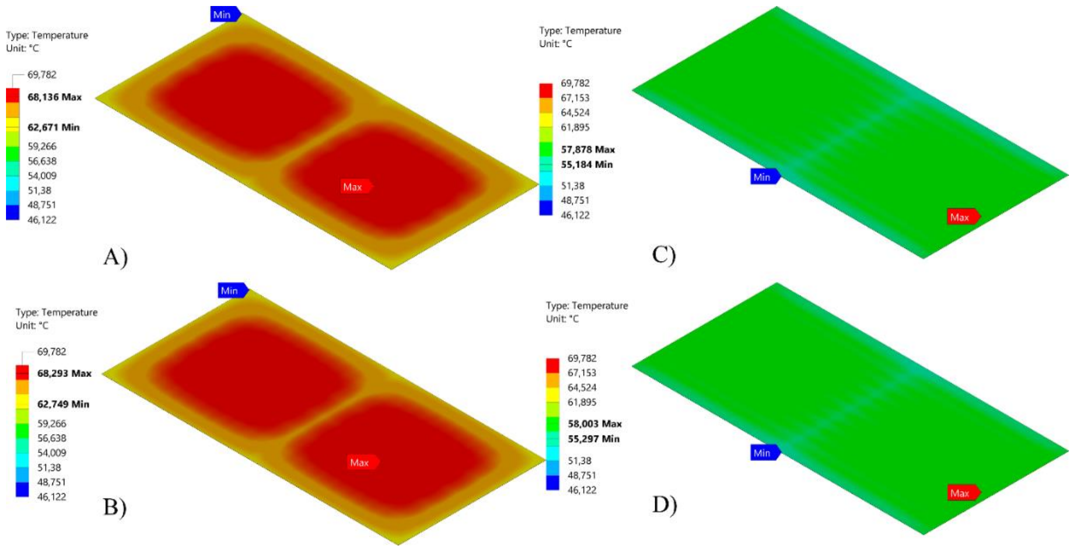

Figure 10**.** Steady-state temperature contour maps of the aluminum backsheet for PV Panel 2, PV Panel 3, PV panel 4 and PV Panel 5. The same color scale is used for both panels to allow direct comparison.

Impact of Thermal Management on Electrical Performance

As illustrated in the temperature distribution contours in Figure 5, the vast majority of the solar cells in each design operate at temperatures very close to the maximum values (Tmax}). The lower temperatures are primarily confined to narrow regions near the aluminum frames, which represent a relatively small portion of the total panel surface. Therefore, utilizing Tmax for the efficiency calculations ensures that the performance estimation is both representative of the overall active cell area and remains on the conservative side.

Table 5. Predicted electrical efficiency and performance improvement for different designs.

Configuration	T_c (T_{max}, °C)	Electrical Efficiency (η (%))	Relative Efficiency Gain (%)
PV Panel 1	69.78	17.94	-
PV Panel 2	68.85	18.01	0.39
PV Panel 3	68.68	18.02	0.45
PV Panel 4	58.80	18.76	4.57
PV Panel 5	58.50	18.78	4.68

As demonstrated in the detailed calculation for the reference module (PV Panel 1), the operating temperature of 69.782 °C leads to a significant reduction from the rated efficiency of 21.28% down to 17.94%. While the panel is expected to perform at its rated efficiency of 21.28% under standard test conditions (STC), the increased operating temperatures under the specific environmental conditions of Bitlis result in an actual efficiency of 17.94%. This 15.67% drop in performance highlights the critical thermal challenge that the subsequent designs (PV Panels 2–5) aim to mitigate.

As shown in Table 5, while the standard module (PV Panel 1) operates at an efficiency of 17.94% due to high thermal losses, the integration of angled fins in PV Panel 5 increases this value to 18.78%. This represents a 4.68% relative improvement in electrical performance. These findings confirm that the significant reduction in peak cell temperature directly translates into a higher energy yield, justifying the implementation of the finned backsheet design for enhanced PV performance.

Comparison of Design Weights

The calculated total masses of the photovoltaic panels were 26.54 kg for PV Panel 1, 33.519 kg for PV Panel 2, 32.466 kg for PV Panel 3, 40.849 kg for PV Panel 4, and 39.797 kg for PV Panel 5. According to steady-state thermal analysis in ANSYS, the integration of aluminum backsheet and angled fin structures contributed to a noticeable reduction in panel temperature; however, this improvement was accompanied by a significant increase in mass. Since mass is also a critical parameter for photovoltaic modules—affecting installation, mechanical stability, and system design—the temperature benefits must be evaluated together with the added weight.

Conclusion

The analysis, based on steady-state thermal analysis in ANSYS, demonstrated that the standard PET-based panel exhibited the highest PV cell temperatures, with maximum and minimum values of 69.782 °C and 60.746 °C, respectively. Adding an aluminum layer as a backsheet to a PET panel provided modest improvement (maximum 68.848 °C, minimum 62.93 °C) by enhancing lateral heat transfer and slightly raising the minimum PV cell temperatures. A panel with only an aluminum backsheet achieved reductions similar to the PET + aluminum configuration, confirming that PET alone has minimal influence on thermal performance. The most significant reductions were observed in finned designs, which minimized both maximum and minimum PV cell temperatures and produced the most uniform thermal distribution. The panel with a PET + aluminum backsheet with angled fins exhibited a maximum of 58.802 °C and a minimum of 55.822 °C, while the panel with only an aluminum backsheet with angled fins exhibited a maximum of 58.503 °C and a minimum of 55.811 °C. These thermal reductions directly translated to an electrical performance boost, where the integration of angled fins raised the panel efficiency from 17.94% to 18.78%, marking a 4.68% relative improvement over the reference module. The finned panel without PET performs nearly the same as the one with PET, further verifying the limited effect of PET when angled fins are present. Overall, integrating angled fins with an aluminum backsheet is one of the most effective approach to reduce localized heating, minimize temperature gradients, and improve the thermal reliability of PV panels. Nevertheless, these thermal improvements come at the cost of increased panel mass, rising from 26.54 kg in the standard PET panel to 39.797 kg in the finned aluminum design, emphasizing the need to balance thermal benefits against installation, mechanical stability, and system design considerations.

Ethical Statement

The author declares that this document does not require ethics committee approval or any special permission.

Conflict of Interest

The authors declare that they have no known competing financial interests or personal relationships that could have appeared to influence the work reported in this paper.

Declaration of Generative AI and AI-assisted technologies in the writing process

During the preparation of this work the author used Al programs in order to improve readability and language. After using this tool/service, the author(s) reviewed and edited the content as needed and take(s) full responsibility for the content of the publication.

References

[1] S. K. Pathak, P. O. Sharma, V. Goel, S. Bhattacharyya, H. Ş. Aybar, and J. P. Meyer, "A detailed review on the performance of photovoltaic/thermal system using various cooling methods," *Sustain. Energy Technol. Assessments*, vol. 51, p. 101844, Jun. 2022.

[2] M. M. Uyar, A. Çıtlak, and A. B. Demirpolat, "Investigation of performance and emission values of new type of fuels obtained by adding MgO nanoparticles to biodiesel fuels produced from waste sunflower and cotton oil," *Ind. Crops Prod.*, vol. 222, p. 119712, 2024.

[3] E. Korkmaz, "Energy demand estimation in Turkey according to modes of transportation: Bezier search differential evolution and black widow optimization algorithms-based model development and application," *Neural Comput. Appl.*, vol. 35, no. 9, pp. 7125–7146, 2023.

[4] A. B. Demirpolat, M. M. Uyar, and A. Çıtlak, "Experimental Investigation of biodiesel fuels obtained by enriching the content of vegetable and waste oils with nanoparticles and modeling of data obtained from the produced fuel samples using artificial intelligence," *Sustain.*, vol. 17, no. 23, pp. 10689, 2025.

[5] S. Shoeibi, H. Kargarsharifabad, M. Sadi, A. Arabkoohsar, and S. A. A. Mirjalily, "A review on using thermoelectric cooling, heating, and electricity generators in solar energy applications," *Sustain. Energy Technol. Assessments*, vol. 52, p. 102105, 2022.

[6] H. Xu, N. Wang, C. Zhang, Z. Qu, and F. Karimi, "Energy conversion performance of a PV/T-PCM system under different thermal regulation strategies," *Energy Convers. Manag.*, vol. 229, p. 113660, 2021.

[7] Y. Sayan, "Investigating the impact of inverted-trapezoidal cross-section flow channels on the performance of a proton exchange membrane fuel cell with a parallel flow channel configuration," *Renew. Energy*, vol. 256, p. 124001, 2026.

[8] A. Yildiz, G. Cakmak, and Y. Bilgic, "Assessment of energy and exergy efficiencies of mini photovoltaic modules," *Int. J. Exergy*, vol. 44, no. 3-4, 2024.

[9] M. A. Akrouch, K. Chahine, J. Faraj, F. Hachem, C. Castelain, and M. Khaled, "Advancements in cooling techniques for enhanced efficiency of solar photovoltaic panels: A detailed comprehensive review and innovative classification," *Energy Built Environ.*, vol. 6, no. 2, pp. 248–276, 2025.

[10] A. R. Abd Elbar, F. B. Baz, S. A. Marzouk, A. Eldesoukey, and A. M. Salem, "Analyzing solar still performance with PV electricity storage: Energy, exergy, exergoeconomic, and

enviroeconomic perspectives," *Desalination*, vol. 597, p. 118400, 2025.

[11] H. Das, P. Dutta, P. P. Dutta, and P. K. Choudhury, "Experimental analysis of a solar air heater using waste mild steel chips as a sensible heat storage material," *Environ. Sci. Pollut. Res.*, vol. 32, no. 28, pp. 17262–17284, 2024.

[12] A. S. Soliman, P. Cheng, A. A. Sultan, O. Abdelrehim, and M. A. Sultan, "A new design of a bifacial solar air heater with PCM," *Therm. Sci. Eng. Prog.*, vol. 59, p. 103380, 2025.

[13] G. Çakmak and C. Yildiz, "The drying kinetics of seeded grape in solar dryer with PCM-based solar integrated collector," *Food Bioprod. Process.*, vol. 89, no. 2, pp. 103–108, 2011.

[14] P. Rawat and A. F. Sherwani, "Annual assessment of solar air-drying system integrated with photovoltaic and phase change material for cost-effective and efficient productions," *Dry. Technol.*, vol. 43, no. 5, pp. 878–908, 2025.

[15] E. El, G. Çakmak, and C. Yıldız, "Efficiency analysis of tank-type water distillation system integrated with hot water collector," *Therm. Sci. Eng. Prog.*, vol. 3, pp. 24–30, 2017.

[16] Shankaranarayanan. S and D. K. Murugan, "Recent trends in thermal energy storage for enhanced solar still performance," *Renew. Sustain. Energy Rev.*, vol. 212, p. 115373, 2025.

[17] A. Saxena *et al.*, "A thermodynamic review on concentrating type solar cookers," *Sol. Energy*, vol. 286, p. 113159, 2025.

[18] C. Sun, Y. Zou, C. Qin, B. Zhang, and X. Wu, "Temperature effect of photovoltaic cells: a review," *Adv. Compos. Hybrid Mater.*, vol. 5, no. 4, pp. 2675–2699, 2022.

[19] S. Kılıçkap Işık and E. El, "Experimental investigation of distilled water production performance of conventional solar stills using $CaCl_2{\cdot}6H_2O$ phase change material reinforced with $SrCl_2{\cdot}6H_2O$ and graphene-based nanoparticles," *Case Stud. Therm. Eng.*, vol. 62, p. 105184, 2024.

[20] E. El and S. K. Isık, "Enhancing solar distillation efficiency with sodium acetate trihydrate phase change material integrated with graphene-based nanoparticles," *Case Stud. Therm. Eng.*, vol. 75, no. September, pp. 107109, 2025.

[21] K. Bilen and İ. Erdoğan, "Effects of cooling on performance of photovoltaic/thermal (PV/T) solar panels: A comprehensive review," *Sol. Energy*, vol. 262, pp. 111829, 2023.

[22] W. Zhang *et al.*, "Performance analysis of a thermoelectric cooler based on thermal management," *Appl. Therm. Eng.*, vol. 265, p. 125655, 2025.

[23] M. Maksymuk, T. Parashchuk, A. Bohra, W. Nowak, and K. T. Wojciechowski, "Improvement of the solar thermoelectric generator performance using concentrated sunlight," *Appl. Therm. Eng.*, vol. 274, p. 126606, 2025.

[24] D. Dewanjee and B. Kundu, "A review of applications of green nanofluids for performance improvement of solar collectors," *Renew. Energy*, vol. 240, p. 122182, 2025.

[25] H. Shawish, M. Özdenefe, and S. Erdem, "Performance investigation and machine learning modeling of PV panels equipped with PCM based passive cooling systems," *Appl. Therm. Eng.*, vol. 274, p. 126588, 2025.

[26] A. Keçebaş, O. V. Güler, A. G. Georgiev, E. Y. Gürbüz, A. D. Tuncer, and İ. Şahinkesen, "Thermodynamic analysis and efficiency enhancement of PV/T systems using ethanol-based phase change material," *Energy*, vol. 320, p. 135165, 2025.

[27] H. S. Abdelmohsen, A. Alrashedy, S. Abdelhady, and A. Rekaby, "Enhancing PV performance using a novel water jacket and humidified air-cooling systems in arid climates," *Appl. Therm. Eng.*, vol. 278, p. 127259, 2025.

[28] M. A. Bashir and H. M. Ali, "Numerical investigation of passive cooling of the PV module using extended fin heat sinks: A parametric analysis," *Process Saf. Environ. Prot.*, vol. 195, p. 106749, 2025.

[29] A. A. Hasan, M. Abdullah, and A. S. Sazid, "A Computational Analysis of Air-Cooled Heat Sinks Designs for PV Solar Panel Cooling With Different Fin Numbers," *Heat Transf.*, vol. 54, no. 2, pp. 1462–1475, 2025.

[30] A. S. Soliman and P. Cheng, "A new heat sink for cooling photovoltaic systems using fins filled with multiple PCMs," *J. Energy Storage*, vol. 114, p. 115875, 2025.

[31] A. Saxena, N. Agarwal, and B. Norton, "Design and performance characteristics of an innovative heat sink structure with phase change material for cooling of photovoltaic system," *Energy Sources, Part A Recover. Util. Environ. Eff.*, vol. 47, no. 1, pp. 10721–10745, 2025.

[32] I. Hossain, A. T. Ngoupo, S. Bhattarai, S. P. Challagulla, and S. K. Sharma, "Empirical survey on the effect of straight and wavy fins integrated with wind stream as heat sink of photovoltaic panels," *Int. J. Environ. Sci. Technol.*, vol. 22, no. 4, pp. 2479–2492, 2025.

[33] TommaTech, "144PM10 550-530Wp Black&White Series Güneş Panelleri.pdf," 2025. [Online]. Available: https://tommatech.de/tr/urun/tommatech-550wp-m10-144pm-hc-mb-gunes-paneli-725.html. [Accessed: 20-Apr-2025].

[34] "Sunmax premium range (Arsenic- and antimony-free ultra low-iron float glass for solar applications)," *AGC Glass Europe*, 2025. [Online]. Available: https://www.agc-yourglass.com/sites/default/files/2022-02/Factsheet_SunmaxPremium-solar-applications_0122_EN.pdf. [Accessed: 05-May-2025].

[35] I. Lamaamar, A. Tilioua, Z. Benzaid, A. A. Msaad, and M. A. H. Alaoui, "Heat transfer study of poly-c PV system integrated with phase change material under semi-arid area (Errachidia- Drâa Tafilalet)," *E3S Web Conf.*, vol. 297, pp. 01008, 2021.

[36] M. Ahmed and A. Radwan, "Performance evaluation of new modified low-concentrator polycrystalline silicon photovoltaic/thermal systems," *Energy Convers. Manag.*, vol. 149, pp. 593–607, 2017.

[37] A. Pavlovic, C. Fragassa, M. Bertoldi, and V. Mikhnych, "Thermal Behavior of Monocrystalline Silicon Solar Cells: A Numerical and Experimental Investigation on the Module Encapsulation Materials," *J. Appl. Comput. Mech.*, vol. 7, no. 3, pp. 1847–1855, 2021.

[38] "PET white Material data sheet," *WILHELM HERM. MÜLLER*, 2025. [Online]. Available: https://whm.net/wp-content/uploads/2023/09/pet-white.pdf. [Accessed: 17-May-2025].

[39] T. Okada, R. Ishige, and S. Ando, "Analysis of thermal radiation properties of polyimide and polymeric materials based on ATR-IR spectroscopy," *J. Photopolym. Sci. Technol.*, vol. 29, no. 2, pp. 251–254, 2016.

[40] K. J. Geretschläger, G. M. Wallner, and J. Fischer, "Structure and basic properties of photovoltaic module backsheet films," *Sol. Energy Mater. Sol. Cells*, vol. 144, pp. 451–456, 2016.

[41] "CY11 PET Film for Solar Cell Back sheet," *YUXING*, 2025. [Online]. Available: https://www.bopet-film-china.com/tr/Product/CY11-PET-Film-for-Solar-Cell-Back-sheet.html. [Accessed: 14-Jun-2025].

[42] "Aluminum 1050-H14," *MatWeb*. [Online]. Available: https://www.matweb.com/search/datasheet.aspx?matguid=b1aa69c0528a40729478403542a8c94a&n=1&ckck=1. [Accessed: 12-Jun-2025].

[43] Y. A. Çengel, *Isı ve kütle transferi.*, 3rd ed. Güven Kitabevi, 2011.

[44] T. S. Shih, P. S. Wei, and Y. Sen Huang, "Optical properties of anodic aluminum oxide films on Al1050 alloys," *Surf. Coatings Technol.*, vol. 202, no. 14, pp. 3298–3305, 2008.

[45] "Ground reflection," *PV*SOL*, 2025. [Online]. Available: https://help.valentin-software.com/pvsol/en/calculation/irradiation/ground-reflection/. [Accessed: 11-May-2025].

[46] C. B. Honsberg and S. G. Bowden, "PVEDUCATION," 2019. [Online]. Available: https://www.pveducation.org/. [Accessed: 24-Feb-

2025].

[47] LATITUDE, “GPS coordinates of Bitlis, Turkey.” [Online]. Available: https://latitude.to/map/tr/turkey/cities/bitlis. [Accessed: 15-Apr-2025].

[48] B. D. Perovic, J. L. Klimenta, D. S. Tasic, J. L.G. Peuteman, D. O. Klimenta, and L. N. Andjelkovic, “Modeling the effect of the inclination angle on natural convection from a flat plate: The case of a photovoltaic module,” *Therm. Sci.*, vol. 21, no.2, pp.925-938, 2017.

[49] S. Armstrong and W. G. Hurley, “A thermal model for photovoltaic panels under varying atmospheric conditions,” *Appl. Therm. Eng.*, vol. 30, no. 11–12, pp. 1488–1495, 2010.

[50] D. L. Evans, “Simplified method for predicting photovoltaic array output,” *Sol. energy*, vol. 27, no. 6, pp. 555–560, 1981.

[51] E. Skoplaki and J. A. Palyvos, “On the temperature dependence of photovoltaic module electrical performance: A review of efficiency/power correlations,” *Sol. Energy*, vol. 83, no. 5, pp. 614–624, 2009.

[52] “Turkish State Meteorological Service.” [Online]. Available: https://www.mgm.gov.tr/eng/forecast-cities.aspx?m=BITLIS. [Accessed: 26-Apr-2025].

[53] F. ORAL, “Bitlis İlinin Rüzgâr Enerjisi Potansiyelinin İstatistiksel Analizi,” *DÜMF Mühendislik Derg.*, vol. 11, no. 2, pp. 671–678, 2020.